Acta Biomaterialia 202 (2025) 545–558

Contents lists available at ScienceDirect

Acta Biomaterialia

journal homepage: www.elsevier.com/locate/actbio

Full length article

Self-emulsifying drug delivery systems: A comparison of dry and wet reverse micelles

Numan Eczacioglu [a,b], Annika Postina [a], Melanie Ebert [a], Flavia Laffleur [a], Gergely Kali [a], Anna Seybold [c], Andreas Bernkop-Schnürch [a,*]

[a] Department of Pharmaceutical Technology, Institute of Pharmacy, University of Innsbruck, Innrain 80/82, Innsbruck 6020, Austria
[b] Department of Bioengineering, Karamanoğlu Mehmetbey University, 70110 Karaman, Türkiye
[c] Department of Zoology, University of Innsbruck, 6020 Innsbruck, Austria

ARTICLE INFO

Keywords:
SEDDS
Dry reverse micelles
Wet reverse micelles
Cellular uptake
Transwell permeability
Bioavailability

ABSTRACT

This study aimed to compare the performance of dry reverse micelles (dRMs) and wet reverse micelles (wRMs) in self-emulsifying drug delivery systems (SEDDS). Reverse micelles (RMs) were formed using cationic, amphoteric, and non-ionic surfactants with various model dyes incorporated into these RMs. Reverse critical micellar concentration (rCMC), entrapment efficiency (EE), and partition coefficients (logD) were determined. SEDDS were loaded with RMs, and their size distributions, polydispersity index (PDI), and zeta potential were evaluated. Cytotoxicity levels, cellular uptake, and membrane permeability of Caco-2 cells were tested. Furthermore, horseradish peroxidase (HRP) loaded SEDDS-RMs were administered to rats, and plasma HRP concentration and bioavailability were determined. Sorbitan monooleate-based dRMs exhibited an rCMC of 0.95 % and 0.6 % for wRMs, with R values of 4.7 and 43.2, respectively. The lower the hydrophilic lipophilic balance (HLB) of the oily phase, the lower the water uptake capacity of reverse micelles. Incorporating methylene blue into dRMs resulted in a logD of 1.56 and an EE of 97 %, compared to 0.59 and 74 % in wRMs. Cytotoxicity studies revealed over 90 % cell survival at concentrations up to 0.5 % for SEDDS-dRMs, while SEDDS-wRMs caused complete cell death at concentrations exceeding 0.4 %. Transwell diffusion studies showed that SEDDS-dRMs and SEDDS-wRMs enhanced membrane permeability by 7.5- and 13.5-fold, respectively. SEDDS containing HRP-loaded dry and wet reverse micelles provided an oral bioavailability of 11.2 % and 7.9 % in rats, respectively. Conclusion: Due to their ability to achieve higher logD, enhance encapsulation efficiency, and improve the oral bioavailability of a model protein, dRMs are favored over wRMs in SEDDS.

Statement of significance: Although several strategies have been proposed to improve the bioavailability of peptide-based drugs, challenges related to stability and oral bioavailability still remain. Reverse micelles, which are nanoscale structures, have great potential with advantages such as high encapsulation efficiency, protection against enzymatic degradation, and increased permeability across biological membranes. This study presents a comparative evaluation of dry and wet reverse micelles in self-emulsifying drug delivery systems. The findings highlight that reverse micelles are a promising nanocarrier system for enhancing drug solubility, stability, and cellular permeability, ultimately contributing to more effective oral drug delivery strategies. This advancement could significantly pave the way for optimizing reverse micelle-based formulations for biomedical applications, especially in protein and peptide therapeutics.

Abbreviations

RMs	Reverse micelles
dRMs	Dry reverse micelles
wRMs	Wet reverse micelles
SEDDS	Self-emulsifying drug delivery system
rCMC	Reverse critical micellar concentration
SEDDS-dRMs	Dry reverse micelles anchored self-emulsifying drug delivery system
SEDDS-wRMs	Wet reverse micelles anchored self-emulsifying drug delivery system
MCT	Miglyol 812 (medium-chain triglycerides)

* Corresponding author.
E-mail address: andreas.bernkop@uibk.ac.at (A. Bernkop-Schnürch).

https://doi.org/10.1016/j.actbio.2025.07.027
Received 21 March 2025; Received in revised form 10 July 2025; Accepted 11 July 2025
Available online 12 July 2025
1742-7061/© 2025 The Author(s). Published by Elsevier Inc. on behalf of Acta Materialia Inc. This is an open access article under the CC BY license (http://creativecommons.org/licenses/by/4.0/).

MCM	Capmul MCM C8 EP/NF (mono- and diglycerides of caprylic acid)
MCM/MCT	Mixture of MCT and MCM (1:1, w/w)
RMs-isocetyl stereate	Reverse micelles formed in isocetyl stereate
RMs- MCM/MCT	Reverse micelles formed in MCM/MCT
CB	Cascade blue
FSS	Fluorescein sodium salt
BG	Bromocresol green
MB	Methylene blue
MO	Methylene orange
SL	Soy lecithin
DDAB	Didecyl dimethyl ammonium bromide
GMO	1-oleoyl-rac-glycerol
EE	Entrapment efficiency
PDI	Polydispersity index
TCNQ	7,7,8,8-tetracyanoquinodimethane
HLB	Hydrophilic lipophilic balance
HBSS	Hanks' balanced salt solution
RMFI	Relative mean fluorescence intensity
OPD	o- phenylenediamine dihydrochloride
HRP	Horseradish peroxidase
SGF	Simulated gastric fluid
SIF	Simulated intestinal fluid

1. Introduction

Biopharmaceutical classification system (BCS) class-III drugs are hydrophilic compounds with high solubility in gastrointestinal (GI) fluids but poor permeability of mucosal membranes [1]. For oral delivery of these drugs, various strategies such as the use of permeation enhancers and efflux pump inhibitors have been developed. Recently, lipid-based nanocarriers containing lipophilic complexes of these drugs have emerged as new approaches to enhance their oral bioavailability. In particular, self-emulsifying drug delivery systems (SEDDS) have attracted the pharmaceutical industry, as the scale-up and production of such nanocarriers is comparatively simple and less cost-intensive. The use of SEDDS offers a promising strategy to protect incorporated drugs from harsh pH conditions and degradation by gastrointestinal enzymes. Furthermore, SEDDS can improve the cellular uptake of their cargo. However, forming highly lipophilic complexes to properly embed hydrophilic drugs in these lipid-based nanocarriers is challenging.

The aqueous or solvent-containing systems enable the incorporation of large amounts of hydrophilic drugs. However, problems such as storage stability due to hydrolytic cleavage of peptide drugs and poor intestinal membrane permeability should be considered. In order to overcome these obstacles, methods to increase the lipophilicity of the drugs or carrier systems have been investigated [2,3]. By the formation of hydrophobic ion pairs (HIP) the lipophilic character of charged hydrophilic drugs can be improved [4]. Nonetheless, this approach has its shortcomings, as the formation of HIPs depends on anionic or cationic substructures within the drug, and often, the increase in lipophilicity is insufficient.

A promising alternative to HIPs is reverse micelles (RMs). Since the 1980s, they have been utilized for the isolation of biological macromolecules, including proteins and nucleic acids, via liquid-liquid extraction. These colloidal systems, characterized by an aqueous core encased in a hydrophobic shell, offer a classical approach to solubilize hydrophilic compounds in an organic solvent matrix [5–7]. Based on their water uptake capacity, RMs are classified as wet reverse micelles (wRMs) and dry reverse micelles (dRMs). wRMs have larger particle sizes, allowing the incorporation of a high quantity of hydrophilic drugs compared to dry ones [8]. In contrast, dRMs lack water or hydrophilic solvents [9]. Techniques such as the lyophilization of wRMs are employed to form dRMs [10,11]. Although previous studies have outlined the dynamics and structural characteristics of reverse micelles [5,9,12–16], none have directly compared dry and wet RM systems in the context of enzyme-loaded SEDDS formulations. Considering the known hydrolytic sensitivity of therapeutic peptides and their poor intestinal membrane permeability [17], the use of SEDDS containing RMs presents a formulation advantage by reducing water-induced degradation, thereby enhancing both stability and membrane permeability.

Recent research by our group investigated SEDDS/RM and SEDDS/HIP combinations [18,19]. Sandmeier et al. reported that RMs improved semaglutide's lipophilicity by nearly twofold compared to HIP, resulting in a 4.2-fold higher SEDDS payload. Permeability studies on Caco-2 cell lines showed that SEDDS revealed significantly higher semaglutide permeation across all formulations, highlighting the beneficial role of lipophilic complexes in enhancing semaglutide delivery [19].

However, despite advances in reverse micelle technology, a direct comparison of their properties, particularly between dry and wet reverse micelles, is missing. Hence, the aim of this study was to design and evaluate both dry and wet reverse micelles and to compare their performance in SEDDS. RMs were created using non-ionic, cationic, and amphoteric surfactants in various oily phases to obtain dRMs and wRMs. Key parameters, such as reverse critical micellar concentrations (rCMC) and water uptake capacities, were determined. Various model dyes were incorporated into RMs, and the entrapment efficiency (EE) and logD of dyes were determined. SEDDS formulation loaded with RMs was developed and characterized regarding size, polydispersity index (PDI), zeta potential, payload, and dye release. Cellular uptake and permeation studies of SEDDS containing these RMs were conducted on Caco2 cells. Finally, horseradish peroxidase (HRP)-loaded SEDDS-RMs were administered to rats, and the plasma HRP concentration, along with bioavailability, was evaluated using enzyme-linked immunosorbent assay (ELISA).

2. Experimental section

2.1. Materials

Polyethylene glycol oleyl ether (Brij 93, average Mn ~357), didecyl dimethyl ammonium bromide (98 %), 1-oleoyl-rac-glycerol, n-octanol (99 %), bromocresol green, fluorescein sodium salt, methylene blue, methyl orange, safranin-o, dialyses tubing cellulose membrane and 7,7,8,8-tetracyanoquinodimethane (98 %) were obtained from Sigma-Aldrich (Steinheim, Germany). Cascade blue™ hydrazide trilithium salt, horseradish peroxidase (HRP, ≥85 units per mg dry weight) and QuantaRed™ Enhanced Chemifluorescent HRP Substrate (ELISA kit) were purchased from Thermo Scientific. Soy lecithin (Lipoid S 100, phosphatidylcholine, content ≥ 94.0 %) was a gift from Lipoid GmbH (Ludwigshafen, Germany). Miglyol 812 (medium-chain triglycerides - MCT) was supplied by Caelo (Hilden, Germany). Capmul MCM C8 EP/NF (mono- and diglycerides of caprylic acid - MCM) was a gift from Abitec Corporation (Janesville (WI), USA). Sorbitan monooleate (Span 80) was obtained from Carl Roth (Karlsruhe, Germany). Isocetyl stearate was supplied by Crodamol (Yorkshire, UK). Cell culture materials were supplied by Biochrom GmbH (Germany), and other chemicals and reagents were obtained from commercial sources. HPLC quality water and solvents were obtained from VWR (Vienna, Austria).

2.2. Formation of reverse micelles

Reverse critical micellar concentration (rCMC) of polyethylene glycol oleyl ether, didecyl dimethyl ammonium bromide (DDAB), soy lecithin (SL), and sorbitan monooleate was determined by the dye solubilization method using 7,7,8,8-tetracyanoquinodimethane (TCNQ) as the indicator for oil-soluble surfactants in non-aqueous media. These surfactants were selected for their ability to form nanoemulsions at low HLB and their safety profiles as approved excipients in oral drug delivery. Oily phases were used due to their generally recognized as safe (GRAS) status, compatibility with oral delivery, and high solubilization capacity for lipophilic drugs.

Oily stock solutions, comprising 5 % (w/w) of polyethylene glycol oleyl ether, SL, and sorbitan monooleate, and 1 % (w/w) of DDAB in each oily phase (isocetyl stearate, n-octanol, MCT, and MCT/MCM (1:1, w/w)) were meticulously prepared. Following homogenization through vortex mixing, the solutions were subjected to ultrasound treatment (Bandelin Sonorex, Germany) for 2 min. The incubation process was executed at 1500 rpm and 70 °C for 3 h using a Thermomixer C (Eppendorf ThermoMixer® C, Eppendorf AG, Germany) to ensure complete dissolution of the surfactants in the oily phase.

Subsequently, oily stock solutions prepared in isocetyl stearate and MCT/MCM were diluted to obtain a surfactant concentration range of 0.005 % to 5 %. To 0.2 mL of each dilution, 0.2 mg (~0.6 μmol) of dye was added. After vortex mixing and ultrasonic treatment for 3–5 min, the samples were shaken vigorously at 1500 rpm for 24 h on a Thermomixer C at 37 °C, leading to TCNQ containing RMs. Undissolved dye was separated by centrifugation at 13,400 rpm for 20 min. Aliquots of 100 μL were withdrawn from the supernatant, and the absorbance of solubilized dye was measured using a microplate reader (Tecan; Salzburg, Austria). The rCMCs were determined as the inflection points of the curves obtained at a wavelength of 480 or 850 nm for TCNQ against the logarithm of surfactant concentrations, with plain oil serving as a reference.

The water uptake of reverse micelles was investigated for each oily phase and surfactant, following a previously established method with minor changes [18]. In brief, demineralized water was titrated in increments of 1 μL to the surfactant-in-oil solution (surfactant concentration range of 0.005 % to 5 %). After the addition of each aliquot of water, samples were homogenized by vortex mixing and subjected to ultrasonic treatment for 2–3 min, followed by an incubation period of 15–30 min. The addition of water was continued until the samples had a cloudy or milky appearance, or water droplets were observed at the bottom of the Eppendorf tubes. By the same method, the water uptake capacity of plain oily phases was determined.

The water-to-surfactant molar ratio (w_0 *or* R value) of the solution was calculated with Eq. (1). This equation can be used to differentiate between dry and wet reverse micelles.

$$R = \frac{[H_2O]}{[Surfactant]} \tag{1}$$

Furthermore, the water content of reverse micelles was determined by NMR spectroscopy. The ^{1}H NMR measurements were performed on a "Mars" 400 MHz Avance 4 Neo spectrometer from Bruker Corporation (Billerica, MA, USA, 400 MHz) in dimethyl sulfoxide-d_6 (DMSO-d_6) solution with the addition of 5 % (m/m) *N,N*-dimethylformamide (DMS), and utilizing prolonged relaxation delay (D1=10 s). The mass percentage of water in the reverse micelle systems was calculated based on the integral values of the methine proton of DMF and water by the following Eq. (2):

$$X_{H_2O(m/m\%)} = \left(0.5 * \left(I_{H_2O,\ 3.33\ ppm} \,/\, I_{DMF,\ 7.95\ ppm}\right) * M_{H_2O} / m_{sample}\right) * 100 \tag{2}$$

where $I_{H_2O,\ 3.33\ ppm}$ and $I_{DMF,\ 7.95\ ppm}$ are the integral values of water at 3.33 ppm and DMF at 7.95 ppm, M_{H_2O} is the molar mass of water, and m_{sample} is the mass of the sample in grams. For sample preparation, an appropriate amount of water was added to RMs to saturate them to their water uptake capacity according to their R values. Samples were also centrifuged to remove water that was not taken up by micelles.

Ruckenstein and Karpe (1990) have calculated the average radius of the inner water cavity of reverse micelles [20]. With the help of this calculation, Azevedo et al. (2000) studied the behavior of AOT reverse micelles models and applied k value of 0.164 nm for AOT [21]. In a similar approach, the average radius of the inner cavity of reverse micelles (r_{RMs}) can be calculated using Eq. (3).

$$r_{RMs}\ (nm) = k \times\ w_0 \tag{3}$$

where k is a proportionality constant that depends on the surfactant and system. The proportionality constant of sorbitan monooleate is not explicitly defined in the literature as a singular constant. Given the relatively high viscosity and long-chain structure of our oily phases (isocetyl stearate and MCT/MCM) compared to lighter oils (*e.g.*, isooctane as used by Azevedo et al.), the proportionality constant may be slightly lower due to reduced micelle dynamics and mobility. It should be in the range of 0.05–0.15 nm, depending on the oily phase and system conditions. In our system, we accepted it as 0.15 nm.

2.3. Dye experiments

An excess amount of bromocresol green (BG), fluorescein sodium salt (a fluorescent dye, FSS), methylene blue (MB), methyl orange (MO), and safranin-O was added to RMs formed with isocetyl stearate (RMs-isocetyl stearate) and MCT/MCM (RMs-MCT/MCM) that were prepared with surfactants in different concentrations (below, around, and above rCMC). They were mixed by vortexing, sonicated for 3–5 min, and left for homogenization overnight in a thermomixer at 1500 rpm and 37 °C. Then, an appropriate amount of water around the water uptake ratios, 1 % for RMs-isocetyl stearate and 20 % for RMs-MCT/MCM was added. The remaining undissolved dyes were removed by centrifugation at 13,400 rpm for 5 min.

Depending on the R values, ^{1}H NMR results, and dye solubility experiments, we referred to RMs-isocetyl stearate formed with sorbitan monooleate as dRMs and RMs-MCT/MCM formed with sorbitan monooleate as wRMs. The solubility of dyes was tested via the same method as described above, and RMs prepared with the 1-oleoyl-rac-glycerol (GMO) as another surfactant with a similar structure to sorbitan monooleate.

The payload of MB was determined for the dRMs and wRMs. Calibration curves were established using MB dilutions in ethanol, with absorbance measured at 668 nm. A slightly modified dry-addition technique was applied to dissolve the dyes in the RMs [22]. The excess amount of dry dye powder was added to both dry and wet RMs. To ensure the entire dissolution, the mixtures were incubated for 12 h at 1500 rpm and 37 °C after sonication for 1 hour. Samples were centrifuged for 20 min at 13,400 rpm to collect the undissolved dyes. The precipitated dyes were first dissolved in ethanol to determine the amount that remained undissolved. After measuring absorbance, the amount of undissolved dye was calculated using a calibration curve. The amount of dye incorporated in the reverse micelles was determined by calculating the difference between the initially incubated amount of dye and the insolubilized dye, and recorded as the maximum payload.

The entrapment efficiencies (EE) were determined using the calibration curve method. The calibration curve for MB in water was established ($R^2 > 0.99$) using a microplate reader as described above. EE of dye was calculated by at first certain amount of MB was dissolved in both dry and wet RMs and underlain with an aqueous phase of demineralized water (w/w, 1:1). Afterwards, the samples were kept in the thermomixer at 37 °C and 300 rpm for 24 h to reach equilibration, followed by centrifugation at 13,400 rpm for 20 min to ensure complete phase separation. Aliquots of 100 μL were withdrawn from the aqueous phase and analyzed by measuring the absorbance of dye contents. The entrapment efficiency of the dye was calculated using Eq. (4). Basically, the equation relies on the difference between the MB concentration in the oily phase at the beginning ($C_{dye-RMs}$) and that released into the aqueous phase in the final state ($C_{dye\ in\ water}$).

$$EE = \frac{C_{dye-RMs} - C_{dye\ in\ water}}{C_{dye-RMs}} \times\ 100 \tag{4}$$

Log D value was calculated using Eq. (5).

$$\log D = \log\left(\frac{C_{dye-RMs}}{C_{dye\ in\ water}}\right) \tag{5}$$

2.4. Preparation of HRP-loaded RMs

HRP was encapsulated within both reverse micelles prior to its incorporation into SEDDS. HRP-loaded RMs were prepared by the dry addition method. Briefly, HRP powder was added directly to the reverse micelles. Afterwards, 1 hour sonication was applied to reach complete solubilization of HRP in the RMs core. Centrifugation at 13,400 rpm was performed to remove undissolved HRP residues.

The concentration of encapsulated HRP molecules in dRMs and wRMs was quantified using a high-performance liquid chromatography (HPLC) system as described below. A XBridge ™ C8 column (130 Å, 3.5 μm, 150 × 4.6 mm) with a security guard column was used. The mobile phases consisted of 0.1 % (v/v) trifluoroacetic acid (TFA) in water/acetonitrile (v/v, 60:40) at a flow rate of 0.8 mL/min. The volume injected was 100 μL, and the detection wavelength was 220 nm with a retention time of 5.4 min. Payloads were determined from the calibration curve, established by HPLC.

2.5. Preparation of self-emulsifying drug delivery systems with empty and loaded RMs

The prepared dRMs and wRMs were loaded with dye and HRP as described above. SEDDS were formed by preparing a pre-concentrate followed by emulsification. For the pre-concentrates (Supplementary Material Table S2), 10 % Chremephor ®EL, 20 % Capryol 90, and 20 % isopropanol were homogenized by shaking at 1500 rpm at 37 °C for 1 hour. This mixture and reverse micelles (empty or loaded) were homogenized at a 1:1 (w/w) ratio. After vortexing to ensure homogenization, pre-concentrates were shaken at 1500 rpm for 1 hour at 37 °C. Afterwards, SEDDS-dRMs and SEDDS-wRMs were emulsified in demineralized water, resulting in the formation of nano-emulsions. The size distribution of reverse micelles and SEDDS formulations containing reverse micelles was measured using dynamic light scattering (DLS). Further morphological evaluation was conducted using energy-filtered transmission electron microscopy (EFTEM) to visualize the structural features of the SEDDS containing reverse micelles [23]. SEDDS samples containing reverse micelles were prepared at 0,5 % (v/v) in demineralized water and subsequently transferred to 200-mesh Formvar/carbon-coated copper grids (Balzers Union, Liechtenstein). After drying, SEDDS containing reverse micelles were analyzed by a Zeiss Libra 120 (Carl Zeiss AG, Oberkochen, Germany). EFTEM images were taken by a 2 × 2 k high-speed camera (Troendle, Germany) and ImageSP software (Troendle, Germany).

2.6. Dialysis studies

Dialysis studies with SEDDSs were performed to determine whether the dye remained stable in RMs. In order to minimize the interaction of the dialysis membrane with the dye, the dialysis membrane used in the study was pre-treated. Dialysis membrane with a molecular weight cut-off of 14 kDa was soaked in a solution of NaCl (10 %) for 24 h, followed by rinsing with demineralized water to remove NaCl residues. The dialysis membrane was then saturated in MB solution for 30 min to reduce dye absorption capacity of the membrane. In order to remove the excess dye that did not adsorb to the membrane, it was incubated in demineralized water until the water remained clear after repeated refreshes.

Dialysis was performed for MB loaded SEDDS-dRMs and SEDDS-wRMs. Also, solubilized MB in water was used as a control. The absorbance of dyes diffusing through the membrane was measured over five hours to determine their release using a microplate reader. The empty saturated membrane was used as a blank. The same procedure was carried out using simulated gastric fluid (SGF, pH 1.2) and simulated intestinal fluid (SIF, pH 6.8) (Supplementary Material Table S4) to investigate the release in the biorelevant environments. The amount of released MB was calculated for both dry and wet systems based on the calibration curve in the relevant media.

2.7. HRP activity determination

HRP activity was determined according to a previously established method with some modification [24]. A substrate solution was prepared by mixing 24 mg of o- phenylenediamine dihydrochloride (OPD), 2.4 mL of 1 M phosphate buffer (pH 6.5), 24 μL of H_2O_2, and 9.6 mL of water. 50 μL of substrate solution, mixed with 350 μL of phosphate buffer and 50 μL of HRP-loaded SEDDS-RMs were added. The enzymatic reaction was carried out at room temperature for 5 min and stopped by the addition of 50 μL of 1 M HCl. HRP activity was determined by monitoring the increase in absorbance of the reaction mixture at 428 nm and plotted as absorbance change per minute.

2.8. Cell viability and hemolysis studies

Empty SEDDS-dRMs and SEDDS-wRMs were prepared as described above with a slight modification in the emulsification step, using Hanks' Balanced Salt Solution (HBSS) buffer instead of demineralized water for the treatment of cells.

Caco-2 cell viability was evaluated by resazurin assay. Resorufin is a pink and fluorescent end product of the metabolism of resazurin by viable cells. For the experiment, Caco-2 cells were seeded on 96 well plate and fed with Red-MEM for 3–4 days. On the day of the experiment, cells were washed with sterile HBSS buffer twice, and then the buffer was removed. 100 μL of each sample was added to wells, and 0.1 % Triton X-100 was applied as a negative control, while HBSS buffer was used as a positive control. The cells were incubated with samples (0.1 to 1 % v/v, SEDDS nanoemulsions) for 4 h at 37°C and washed with sterile HBSS buffer. 150 μL of resazurin was applied to cells and incubated for 3 h in the dark. Aliquots of 100 μL were transferred to black well plate to measure fluorescence intensity (FI) at an emission wavelength of 590 nm of resorufin when excited at 540 nm. Cell viability (%) was calculated according to Equation 6;

$$Cell\ Viability\ (\%) = \frac{FI\ of\ Sample - FI\ of\ TritonX}{FI\ of\ HBSS - FI\ of\ TritonX}\ x\ 100 \quad (6)$$

The hemolytic activity of SEDDS was assessed by measuring hemolysis in erythrocyte concentrates, which were generously provided by Tirol Kliniken GmbH (Innsbruck, Austria). The erythrocyte concentrates were suspended in sterile HEPES-buffered saline (HBS) at a ratio of 1:200. For the experimental procedure, 250 μL of SEDDS, prepared at various concentrations in sterile HBS, was mixed with an equal volume of the diluted erythrocyte suspension, resulting in SEDDS concentrations ranging from 0.125 % to 0.5 % (v/v). Sterile HBS served as negative control, while a 0.5 % (v/v) Triton X-100 solution was used as positive control for hemolysis. Samples were incubated for 3 h at 37 °C and agitated at 100 rpm using an orbital shaker incubator (Orbital Shaker Incubator ES-80, Grant Instruments Ltd, United Kingdom). Following incubation, samples were centrifuged at 2700 rpm for 10 min. Subsequently, 100 μL of the supernatant was transferred to a 96-well microplate, and absorbance at 415 nm was measured using a plate reader (Tecan Spark, Tecan Sales Austria GmbH, Austria). Hemolysis was quantified using the following Eq. (7).

$$Hemolysis\ [\%] = \frac{\text{absorption}_{sample} - \text{absorption}_{negative}}{\text{absorption}_{positive} - \text{absorption}_{negative}} \times\ 100 \quad (7)$$

2.9. In vitro cellular uptake and permeation studies with caco-2 cell monolayer

Fluorescein sodium salt (FSS) was used for cellular uptake studies as a fluorescence marker. Fluorescein-labelled SEDDS were prepared as described above using HBSS buffer to a final non-toxic nanoemulsion

concentration of 0.2 % (v/v). 1.6 μg of FSS was dissolved in sterile HBSS buffer, serving as positive control. Negative control was HBSS buffer.

In vitro cellular uptake study was performed on Caco-2 cells following a previously established method with some minor modifications [25]. Caco-2 cells were seeded at a density of 5×10^4 cells/mL and grown for 11 days. On the day of the experiment, the feeding medium was removed, and cells were washed twice with pre-warmed sterile HBSS buffer. 500 μL of each sample and controls were applied to Caco-2 cells and incubated for 3 h at 37°C. At the end of the exposure period, samples were removed, and cells were washed twice with HBSS buffer to ensure that no sample residue remained. Afterwards, 150 μL of trypsin was added to each well and incubated for 5 min to detach the cells, and the plate was carefully tapped and shaken. 500 μL of Red-MEM was added to quench the trypsin activity. Samples were collected in 15 mL Falcon tubes and centrifuged at 800 rpm for 4 min. Then, supernatant was removed, and cells were washed with sterile phosphate-buffered saline (PBS). PBS was trashed after centrifugation, and 700 μL of sterile PBS was added. After quick and careful resuspension of the cells in PBS, they were filtered through a cell strainer with a pore size of 70 μm. The amount of FSS-loaded SEDDS taken up by Caco-2 cells was quantified via flow cytometry (Attune NxT Flow Cytometer, Thermofisher Scientific). Data were analyzed using FlowJoTM v10.8.1 software. Relative mean fluorescence intensity values (RMFI) were calculated from the mean fluorescence intensity values (MFI) using Eq. (8):

$$RMFI = \frac{MFI_{sample}}{MFI_{buffer}} - 1 \tag{8}$$

Cascade Blue (CB) was used as a fluorescence marker for permeation studies. CB- SEDDS-dRMs and CB- SEDDS-wRMs samples were prepared for *in vitro* permeation study across Caco-2 cell monolayer on transwell plate in the same manner as for *in vitro* cellular uptake studies. The permeation study was performed following a previously established method with some minor modifications [26]. Caco-2 cells were inoculated onto a 24-well transwell plate at a cellular density of 6×10^4 cells/cm^2. The cells were cultured for 21 days, with the culture medium being replenished every alternate day. The Red-MEM exchange with the Opti-MEM was performed 12–24 h prior to the experimental procedure. Permeation study was conducted from the apical to the basolateral compartment.

On the day of the experiment, trans-epithelial electric resistance (TEER) measurements of each well were taken before and after the experiment using an Evom2 apparatus (World Precision Instrument Inc., USA) to ensure the integrity of the cell monolayers. Only cell monolayers with TEER values above 800 Ω.cm^2 were used for the permeation studies. Afterwards, cells underwent a washing step with PBS, followed by equilibration of cell monolayers with HBSS for 30 min. Subsequently, the buffer was aspirated, and 100 μL of the test substance comprising CB was added to the apical compartment. Simultaneously, 500 μL of HBSS was added to the basolateral compartment. Basolateral chamber samples of 100 μL were collected at 30-minute intervals. Following each sampling event, an equivalent volume of HBSS was replenished to maintain a constant volume and sink conditions. The experiment was conducted over a duration of 180 min. CB was dissolved in sterile HBS buffer, serving as positive control. Negative control was HBSS buffer. Quantification of permeated samples was performed by fluorescence measurements (λex = 402 nm and λem = 447 nm) on a microplate reader. Cumulative corrections were made for previously removed samples. The apparent permeability coefficient (Papp) was determined using Eq. (9):

$$P_{app} = \frac{Q}{A \; x \; c \; x \; t} \tag{9}$$

where Q = total permeated sample amount during the time of experiment (mg), A = diffusion area (cm^2), c = initial concentration in the donor chamber (mg/mL) and t = time of experiment (s). Accumulation of CB in the acceptor chamber was plotted as a function of time.

2.10. In vivo HRP experiments

The process received authorization from the Animal Ethical Committee in Vienna, Austria, and conformed to the Principles of Laboratory Animal Care (GZ: 2022–0.792.904). Male Sprague Dawley rats, averaging a body weight between 370 and 470 g, were sourced from Janvier Labs in Le Genest-Saint-Isle, France. Animals were randomly assigned to four groups of three as follows:

1. Oral reference group (Oral HRP administration)
2. Intravenous reference group (Intravenous HRP administration)
3. HRP loaded SEDDS-dRMs group
4. HRP loaded SEDDS-wRMs group

First, the formulations were prepared, including a sterile HRP solution for intravenous administration, HRP solution for oral gavage, HRP-loaded SEDDS (dRMs and wRMs) for oral gavage. On the day of the experiment, SEDDS preconcentrate was diluted (1:10) in HEPES buffer (pH 7.4) to achieve the desired HRP concentration (0.006 mg/mL), and 400 μL of HRP-loaded SEDDS formulations were administered. HRP solution in HEPES buffer for subcutaneous injection was prepared at a concentration of 0.0015 mg/mL.

Blood samples were collected at 30- and 60-minutes intervals over a six-hour period to test the total HRP concentration using the ELISA (QuantaRed™ Enhanced Chemifluorescent HRP Substrate, Thermo Scientific) kit. For sample collection, 100 μL of blood from the tail vein was added to tubes containing 5 μL of 3.6 % (w/v) EDTA solution and vortexed briefly to prevent clotting. The samples were stored on ice and centrifuged at 13,400 rpm for 5 min. The supernatant was stored in the freezer until analysis. For analytical purposes, a calibration curve was constructed by spiking the pre-injection rat sample with HRP solution and serially diluting with water to obtain linear concentrations. Water was used instead of HEPES buffer because HEPES interacts with fluorescence. 10 μL of HRP-loaded solution and blanks were added to a black 96-well plate, followed by 100 μL of HRP substrate enhanced solution. The reaction was stopped after 1 min by adding 10 μL of stop solution. Fluorescence intensity was measured using an excitation wavelength of 570 nm and an emission wavelength of 620 nm. Bioavailability was calculated using the area under the time-dependent change curve of HRP concentration in rat blood.

2.11. Statistical design and analysis of data

All experiments were conducted in triplicate or more, with the results expressed as mean values ± standard deviation (SD). Statistical analysis was carried out using one-way and two-way ANOVA (GraphPad Prism 8), with a significance threshold set at $p < 0.05$. In figures, significance levels are denoted as $^*p < 0.05$, $^{**}p < 0.01$, and $^{***}p < 0.001$.

3. Results and discussion

3.1. Preparation and characterization of reverse micelles

The behavior of reverse micelles such as their size, water uptake capacity, and stability highly depends on the specific surfactant and the non-polar solvent used. Surfactants exhibit different behaviors in solvents according to their ionic strength and chemical structure. Interactions between these components play a crucial role in determining the properties of reverse micelles. In addition, the hydrophilic–lipophilic balance (HLB) of the oily phase plays a crucial role in the formation and properties of RMs. The size of the polar cores in reverse micelles was directly related to the surfactant's HLB value. Therefore, the lower the HLB of the oily phase, the lower the water uptake capacity, which favors the formation of reverse micelles [13]. However, when using oily phases

with low HLB, a sufficiently high solubility of many surfactants cannot be achieved. Prior to application of the surfactants, we conducted preliminary screening to assess their ability to form stable reverse micelles in oily phases. Because of the highly lipophilic nature of the solvent, surfactant selection was limited by their solubility and stability in this non-polar environment. Not all surfactants are compatible with highly lipophilic solvents, so we carefully selected those capable of forming stable reverse micelles under these conditions. The properties of reverse micelles, including size, shape, and stability, are greatly influenced by the nature of the oil phase. The choice of oil influences the interfacial tension, the critical packing parameter, and the hydration of the surfactant headgroups, all of which play a crucial role in determining the reverse micellar properties. By carefully selecting the oil phase and optimizing its composition, it is possible to control the size, shape, and stability of reverse micelles for various applications in fields such as nanotechnology, drug delivery, and catalysis [27–30].

For this study, oily phases with low water uptake capacity and high lipophilicity were preferred to facilitate the formation of dRMs. The availability of surfactants soluble in these oily phases above rCMC needed to form dRMs was limited. The surfactants were solubilized up to a maximum of 5 % in isocetyl stearate. When a mixture of MCT and MCM was used as the oily phase, achieving high solubility was not an issue for any tested surfactants. In order to form reverse micelles, four different surfactants with cationic, nonionic, and amphoteric properties were employed (Fig. 1A). Reverse micelles were formed by dissolving these surfactants in isocetyl stearate and a mixture of MCT with MCM, serving as oily phase for SEDDS. The rCMC for both RMs- isocetyl stearate and RMs-MCT/MCM was determined to be 0.45 % and 0.85 % for polyethylene glycol oleyl ether, 0.14 % and 0.06 % for DDAB, 0.48 % and 0.8 % for SL, and 0.95 % and 0.6 % for sorbitan monooleate, respectively (Fig. 1B-C). These rCMC results are in agreement with several previously published reverse micellar studies [18,31,32]. Supplementary Material Table S1 summarizes rCMC values in the two oily phases.

The water uptake capacity of RMs is highly dependent on the surrounding oily phase. The maximum water pool size is related to the oil used, as the oily phase will penetrate the surfactant interface and increase the hydrocarbon core volume [7]. In addition, the water uptake capacity of the oily phase should be taken into account. The water uptake ratios of RMs formed in oily phases with different water solubilization capacities and R values are shown in Fig. 2. Experimental water uptake capacities of plain oily phases used in this study were determined as <0.05, ~0.4, ~5.7, and ~8 for isocetyl stearate, MCT, and n-octanol, MCT/MCM, respectively.

Subtracting the water solubilization capacities of the oil phases from those of the oily solutions containing RMs shows that the water uptake capacity of the RMs itself is <2.5 %. In particular, the water solubilization study of RMs formed in isocetyl stearate showed that the reverse micelles contain almost no water. As shown in Fig. 2A, the water solubilization capacity is partly dependent on the surfactant concentration.

The water-to-surfactant molar ratio (R) is the key parameter for assessing whether RMs are dry or wet [33]. As there is no specific R value that defines dry and wet RMs in the literature, we defined reverse micelles with $R < 10$ as dry and those with $R > 10$ as wet (Fig. 2B).

The water content of the formed dry and wet reverse micelles was determined via ^{1}H NMR spectroscopy in DMSO-d_6, using 5 % (m/m) DMF as an internal standard (Supplementary Material Figure S1). As shown in Fig. 2C, the water content of dry reverse micelles is negligible, below 1 % (m/m). In case of wet reverse micelles, a significantly higher water content was observed, slightly above 9 % (m/m).

3.2. Dye integration

In general, the more polar a drug is, the better it solubilizes in the core of reverse micelles [7]. So far, reverse micelles have been used to extract many different proteins, including cytochrome-c, lysozyme, α-chymotrypsin, and albumin by utilizing this core [34–37]. The core phase formed by the surfactant provides a more polar environment,

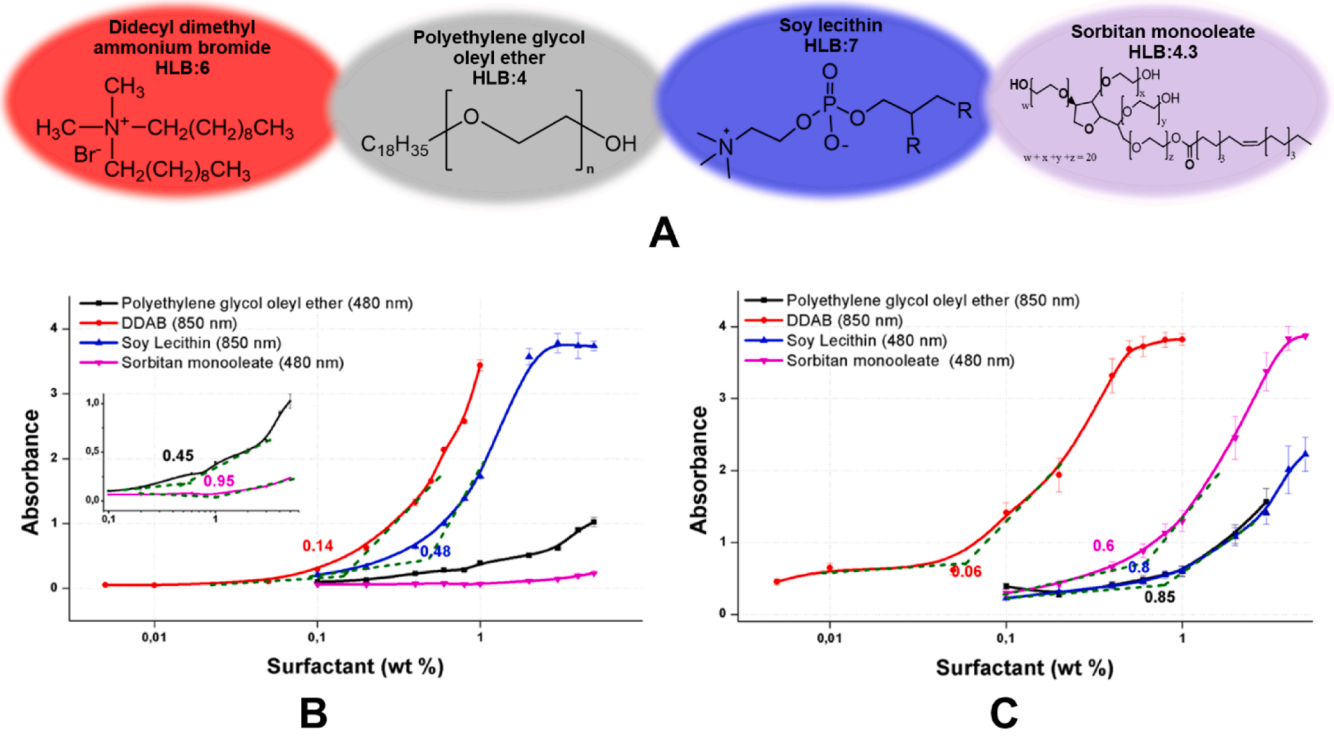


Fig. 1. A. Structures of surfactants used to form RMs – non-ionic: polyethylene glycol oleyl ether, cationic: DDAB, amphoteric: SL and non-ionic: sorbitan monooleate, and rCMCs determination by dye solubilization method with TCNQ; RMs prepared in B. isocetyl stearate, C. in MCT/MCM, Data are shown as means ± SD ($n \geq 3$).

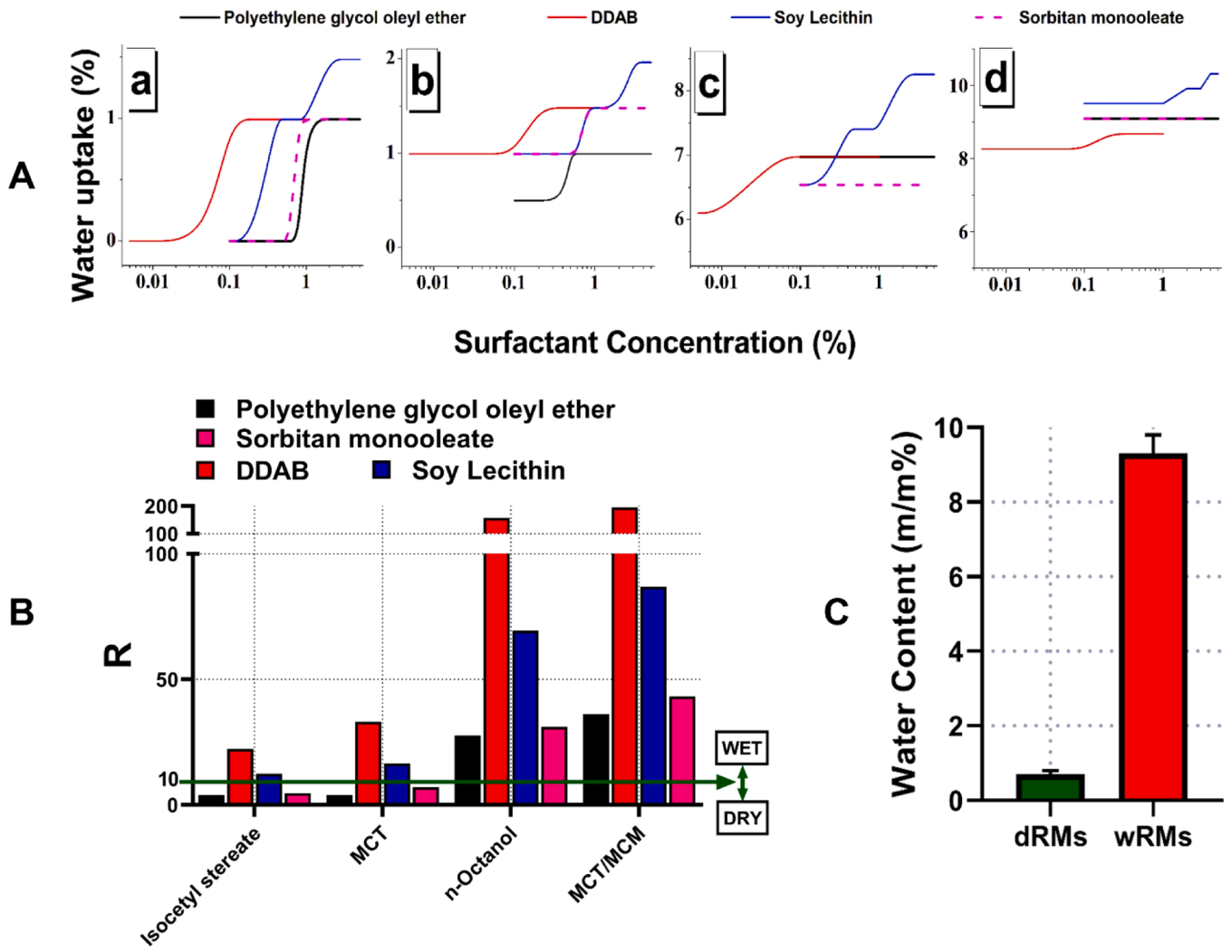


Fig. 2. A. Water uptake percentages of RMs formed in different oily phases as a function of the logarithm of surfactant concentration [wt %]. a. isocetyl stearate, b. MCT, c. n-Octanol, d. MCT/MCM, B. R values of the RMs represent the water-to-surfactant molar ratio, which is defined as the moles of water per mole of surfactant, C. Water content of RMs formed with sorbitan monooleate in isocetyl stearate (dRMs) and MCT/MCM (wRMs) determined by ^{1}H NMR spectroscopy.

allowing molecules to dissolve in it. To confirm that, the dyes can be dissolved in the core of RMs, MB and safranin O were employed as cationic dyes, and MO, BG, and FSS as anionic dyes. The use of different dyes based on charge was included to demonstrate the selective solubilization capabilities of RM systems. The use of diverse dyes allowed us to reveal how reverse micelle components and structure influence the solubilization of various molecules, thereby enabling the proper selection of surfactants for reverse micelle formulation. All dyes were dissolved in RMs-MCT/MCM formed with each surfactant (Fig. 3B). No dye was dissolved in RMs formed with polyethylene glycol oleyl ether in isocetyl stearate, while methyl orange, bromocresol green, and fluorescein sodium salt dyes were dissolved in RMs formed with DDAB and soy lecithin in isocetyl stearate (Fig. 3A). Furthermore, dye solubility may vary with surfactant concentration. Dye solubility in RMs was enhanced with increasing surfactant concentrations. None of the dyes used were soluble in plain isocetyl stearate.

The solubility of dyes in sorbitan monooleate can be attributed to the properties of this surfactant. GMO was also tested to better understand the structural effect on solubilization. Sorbitan monooleate and GMO have similar hydrocarbon chain lengths (oleic acid chain) as steric stability group and two hydroxyls, serving as anchor groups. In GMO, the hydrophilic head group is glycerol, while in sorbitan monooleate, it is sorbitan. Both can form dRMs and dissolve dyes in their core phase. For instance, methylene blue may interact with the hydrophilic head groups of sorbitan monooleate and GMO at the reverse micelle core interface. In case of polyethylene glycol oleyl ether, its lack of a charged group might cause weaker interactions with dyes. This reduced affinity can lead to lower solubility compared to surfactants, where a charged dye interacts with anionic, cationic, or zwitterionic surfactants.

The size and structure of reverse micelles can also influence the solubility of various compounds. The confined space inside the micelles can facilitate the solubilization of certain molecules, like methylene blue. Molecules solubilized in reverse micelles can alter structural properties such as size and shape or water content of reverse micelles and cause conformational changes in molecular-level equilibria at the surfactant interface and in water pools [7]. Some works have even referred to these structures as "*swollen reverse micelles*" [12,38]. Smaller micelles have smaller polar cores, which may limit the amount of polar molecules they can accommodate.

3.3. *Characterization of self-emulsifying drug delivery systems containing RMs*

The maximum MB payload in dRMs was determined to be 1.24 mg/g, while for wRMs it was 5.4 mg/g. This observation can be attributed to the larger size of wRMs compared to dRMs, as also mentioned in the

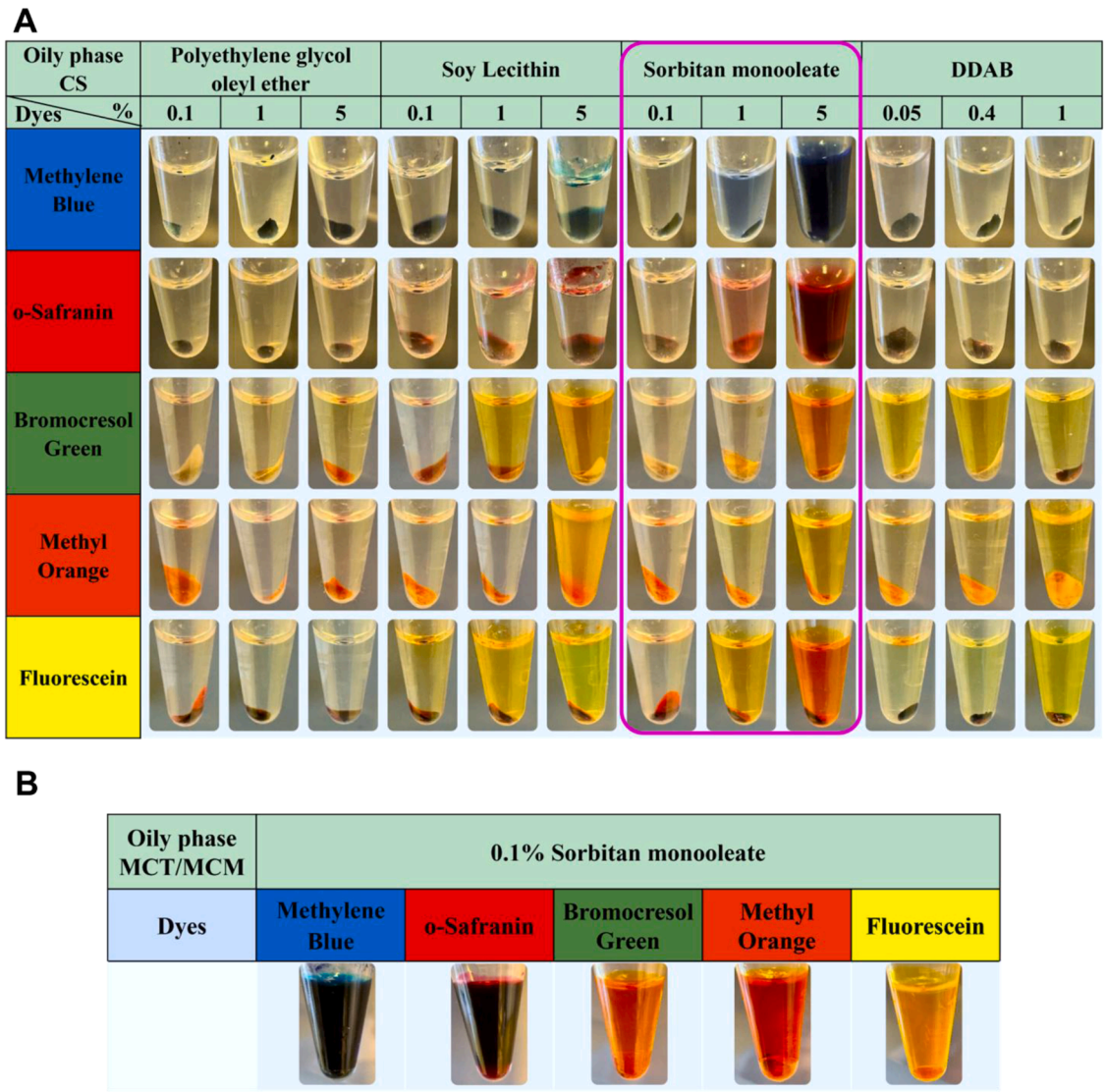


Fig. 3. Cationic dyes (MB and safranin O) and anionic dyes (MO, BG, and FSS) were incorporated in formulations containing indicated surfactants below, around, and above the rCMC in A. isocetyl stearate used as oily phase, B. MCT/MCM used as oily phase.

literature [8]. Another possibility is that MB also dissolves in the plain MCT/MCM used to form wRMs. In the case of dRMs, however, the MB is only involved in the core of the reverse micelles. MB solubilized in the plain MCT/MCM oily phase diffused into the water phase. Therefore, both the entrapment efficiency and Log D of wRMs are lower than those obtained for dry ones (Fig. 5A-B).

The self-emulsifying properties generally depend on environmental factors such as the chemical composition and structure of the surfactants, HLB values, the presence of co-surfactants, and the system's temperature. Oily phase, surfactants, and co-surfactants used for SEDDS play a significant role in creating these chemical compositions. For self-emulsification in oil-in-water systems, it is necessary to use a surfactant with a high HLB value (>14). In the course of the SEDDS, it is important to have a clear phase and avoid any precipitation or phase separation. After testing various formulations that did not mix homogeneously, we developed a formulation that successfully formed SEDDS structures. Experimental results showed that for the pre-concentrate, the molar ratio of Cremophor EL/Capryol 90/Isopropyl alcohol/RMs resulted in a clear transparent phase. The mean droplet size ranged from 96 (SEDDS-wRMs) to 127 nm (SEDDS-dRMs) with a PDI $\leq$ 0.3. The size distribution of dry and wet reverse micelles was further characterized by dynamic light scattering, and the results are provided in the Supplementary Material (Table S3, Figure S3, and Figure S4).

Fig. 4 illustrates the clear difference between SEDDS containing reverse micelles. SEDDS-dRMs exhibit more compact and aggregated features, consistent with dehydrated or low-water-content reverse micelles. The morphology indicates a small internal aqueous phase, potentially affecting drug encapsulation and release profiles. SEDDS-wRMs show distinct, well-dispersed spherical structures, typical of reverse micelles formed in hydrated environments. The relatively uniform size distribution and clear contrast suggest the presence of a stabilized aqueous core. These structural differences highlight the impact of water content on the morphology and internal architecture of reverse micellar formulations within SEDDS platforms. DLS measures the hydrodynamic diameter of particles in solution, while TEM reveals dehydrated particles under high vacuum. Sample preparation and drying can lead to aggregation or deformation, resulting in apparent enlargement and selective visualization of larger structures in TEM.

The zeta potential usually depends on the type of surfactant. Both SEDDS-dRMs and SEDDS-wRMs showed a similar zeta potential, because the surfactant was the same (sorbitan monooleate) (Fig. 5C and Supplementary Material Figure S2). The zeta potential reflects the properties of the surfactant's head group, and since the same surfactant is used, the charge characteristics remain similar across formulations.

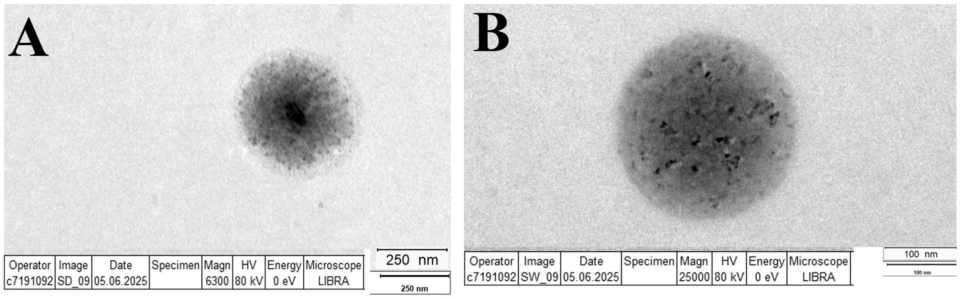


Fig. 4. Energy-filtered transmission electron microscopy images of reverse micellar systems within self-emulsifying drug delivery systems A. SEDDS-dRMs B. SEDDS-wRMs.

Differences may only occur if external factors like pH, ionic strength, or surfactant concentration significantly alter the carrier environment. Variations in the internal core (*e.g.*, water content) or external solvent have little impact on the surface charge density. Even if the size of the micelles or the water content in the core varies across formulations, the surface composition (*i.e.*, surfactant head groups) remains the same. This maintains a consistent electrostatic profile, resulting in similar zeta potential values.

MB in the water was used as a control and was able to release by 75 %. MB release from dRMs-loaded SEDDS did not exceed 8 %, while it reached over 25 % in case of wRMs-loaded SEDDS (Fig. 5D). Since MB can dissolve in the plain MCT/MCM oily phase and exhibits approximately 11 % release. It is challenging to determine whether the released MB originates from the MB entrapped in the wet reverse micelles. However, as MB is not soluble in plain isocetyl stearate, all MB released must be that trapped in dRMs. To evaluate the pH-dependent release profile of methylene blue, SEDDS-dRMs and SEDDS-wRMs were subjected to *in vitro* dialysis in simulated gastric fluid (SGF, pH 1.2) and simulated intestinal fluid (SIF, pH 6.8). As shown in Fig. 5E, the release of MB from both SEDDS systems was negligible under acidic SGF conditions, suggesting high stability of the micellar assemblies and strong retention of the hydrophilic cargo in gastric-like environments. In SIF, a higher cumulative release was observed from SEDDS-dRMs compared to SEDDS-wRMs and free MB (Fig. 5F). This result suggests that SEDDS-dRMs are more prone to release MB at higher pH, potentially due to changes in micellar dynamics, hydration, or core accessibility in intestinal-like environments. The ionic strength and buffer components in SIF may enhance water penetration into the SEDDS-dRMs, disrupting the compactness of the hydrophobic interior. This could decrease the encapsulation efficiency or retention capacity of MB, favoring its release in SIF.

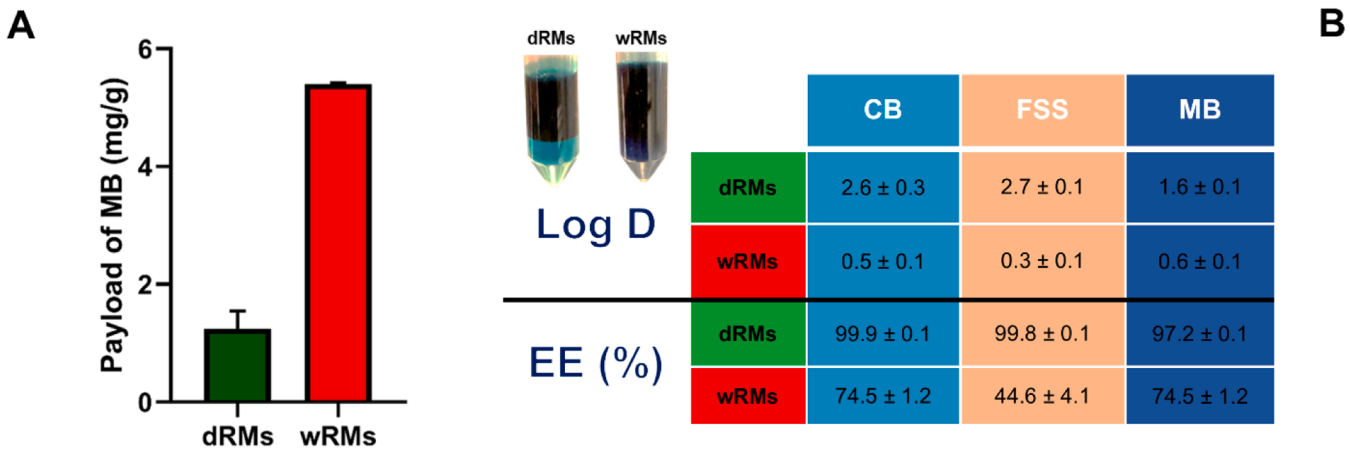
3.4. Cell viability, cellular uptake, and permeability studies with Caco-2 cell line

As cellular uptake and epithelial translocation of SEDDS were examined on Caco-2 cell monolayers, the toxicity level of SEDDS was determined on Caco-2 cells. The viability of Caco-2 cells was tested in the presence of SEDDS emulsion ranging from 0.1 % to 0.5 % v/v. When using SEDDS containing dRMs, a high level of cell survival, exceeding 90 % was observed at concentrations around 0.5 % as illustrated in Fig. 6A. The same level of cell viability was also observed with a 1 % SEDDS formulation containing dRMs. In contrast, wRMs significantly reduced cell viability, with complete cell death observed at concentrations exceeding 0.4 % SEDDS. Surfactant properties, including charge, HLB values, and chemical structures, significantly influence the behavior of reverse micelles. The toxicity of a surfactant is associated with its Gibbs free energy of adsorption and the minimum area it occupies at a surface [39]. The larger particle size of wRMs compared to dRMs may lead to higher Gibbs free energy and different cellular uptake pathways, potentially increasing the likelihood of intracellular stress or toxicity. The presence of water in wRMs makes them more prone to hydrolytic reactions. Furthermore, the higher water content in wRMs can increase the local concentration of surfactants at the interface, which may more easily disrupt cell membranes. Surfactants, particularly at high concentrations, can destabilize lipid bilayers, causing cytotoxic effects.

In addition, hemolytic activity is another method commonly used to assess cytotoxicity. Hemoglobin release correlates with membrane damage and endosomal escape. Hemoglobin release can be assessed in relation to the interaction between SEDDS formulations and the cell membrane. According to the hemolysis assay, SEDDS formulations containing wRMs induced significantly higher hemolysis at all tested concentrations compared to those containing dRMs. At 0.25 % concentration, wRMs caused approximately 80 % hemolysis, while dRMs resulted in <50 % hemolysis (Fig. 6B). Biocompatibility of both dRMs and wRMs was evaluated through cytotoxicity and hemolysis assays. While both systems demonstrated acceptable safety profiles at low concentrations, wRMs exhibited slightly higher cytotoxicity and hemolytic potential at concentrations above 0.3 %. Therefore, the concentration (0.2 %) used in subsequent cellular uptake and epithelial translocation studies was selected based on the threshold where no significant cytotoxic or hemolytic effects were observed.

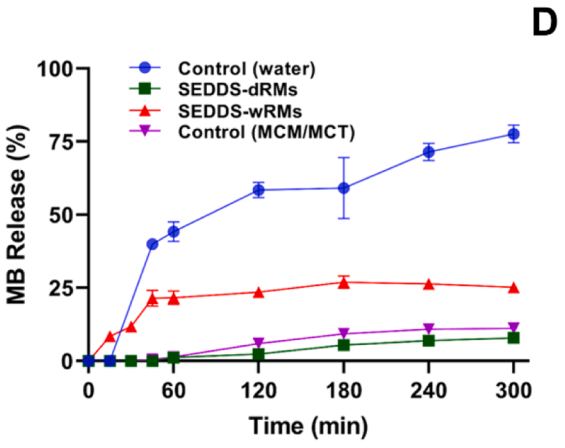
Cellular uptake study on Caco-2 cells was performed utilizing flow cytometry. High cellular uptake is generally characterized by fluorescence shifts to higher values and also higher RMFI values. Flow cytometry histogram in Fig. 6C, obtained after processing the data with FlowJo, shows a prominent shift in the fluorescence intensity distribution of SEDDS towards higher values compared to the control, indicating enhanced cellular uptake. Furthermore, RMFI values show that SEDDS containing wRMs are 1.5 times higher than those containing dRMs (Fig. 6D). The presence of water in wRMs may facilitate higher solubilization of the fluorescent marker, maintain its fluorescence, and therefore, the RMFI value may appear higher. The dye may be more evenly distributed and exposed to the aqueous phase, enhancing its fluorescence. In dry reverse micelles, the absence of water can cause fluorescence quenching of fluorescein sodium salt. The dye may be more confined or trapped within the hydrophobic core, which reduces its fluorescence. Fluorescein exhibits reduced fluorescence in non-aqueous environments, which could explain the lower RMFI in the sample with dry reverse micelles. Nevertheless, analysis of the fluorescence histograms suggests that the extent of the fluorescence shift (which reflects cellular uptake efficiency) was similar between dRM and wRM formulations, indicating comparable levels of internalization despite differences in absolute fluorescence intensity.

To compare the effect of SEDDS containing dRMs and wRMs on transport efficiency, transwell diffusion studies with Caco-2 cell monolayer were performed. Results are shown as a permeation profile over time in Fig. 6E. Cascade blue was preferred as a marker in the permeation study due to its high solubility in water. Moreover, it has excellent fluorescence and, unlike most dyes, resists quenching upon protein conjugation. For these reasons, small molecules such as CB (530 Da) are often used in lab-on-a-chip systems to demonstrate apparent



C

Empty SEDDS	Time (Hour)	Mean Droplet Size [nm]	PDI	Zeta Potential [mV]
dRMs	0	127 ± 8	0.24 ± 0.07	-8.3 ± 2.6
	24	114 ± 6	0.25 ± 0.02	-11.3 ± 0.6
wRMs	0	96 ± 27	0.04 ± 0.02	-6.7 ± 1.6
	24	104 ± 16	0.03 ± 0.02	-8.8 ± 1.5



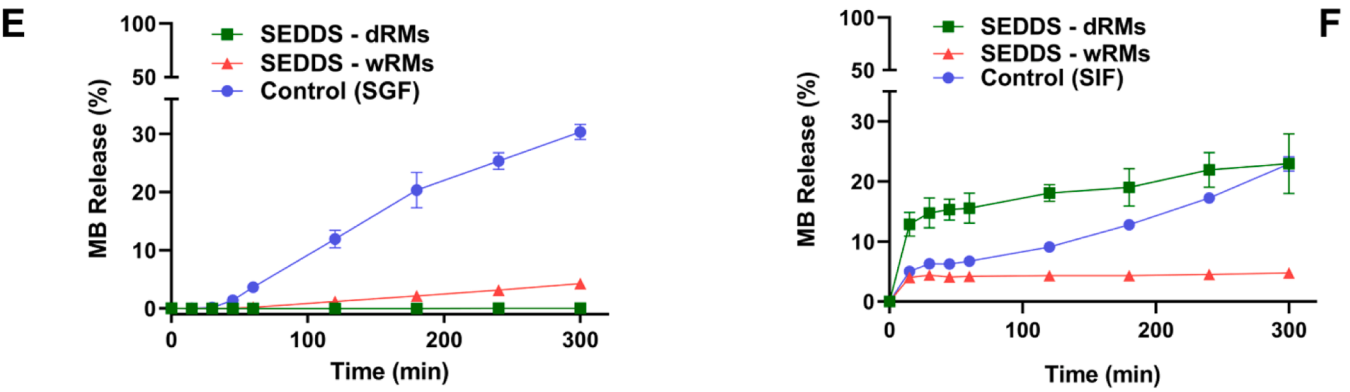


Fig. 5. A. Payload of MB in RMs formed with sorbitan monooleate, B. Log D and EE values of CB, FSS and MB in RMs after 24 h of incubation at 37 °C, C. Droplet size [nm], PDI, and zeta potential [mV] of empty SEDDS dilution (0.5:100) in demineralized water at 37 °C. Cumulative release studies of MB from SEDDS in D. demineralized water, E. simulated gastric fluid (SGF, pH 1.2), and F. simulated intestinal fluid (SIF, pH 6.8) using a dialysis membrane over time. Data are shown as means ± SD ($n \geq 3$).

permeability (P_{app}), which is typically determined to be in the range of 10^{-7} to 10^{-6} cm/s [40–42]. The concentration of CB that permeated the cell monolayer was measured in the effluent, and apparent permeability was calculated using a standard curve (Fig. 6F). SEDDS formulated with dry and wet reverse micelles resulted in 7.5- and 13.5-fold enhanced permeation, respectively. The P_{app} of wRMs was found to be 1.75 times higher than that of dRMs. As highlighted in the dialysis studies, the dye solubilization in the plain oily phase can complicate determining its origin. The dye passing through the cell barrier can originate from wet micelles or from dye dissolved in the oily phase. More dye leaks because it dissolves in the oily phase, rather than due to transport by the micelles. In contrast, for dry reverse micelles, permeation can be entirely attributed to the micelles as the dye is completely trapped inside the hydrophilic core. This distinction suggests that the relatively greater permeability observed with wRMs may, at least in part, result from dye diffusion through the oily phase, rather than solely from micelle-mediated transport alone. Thus, although both systems demonstrated the ability to enhance payload transport across intestinal epithelial models, mechanistic differences arising from micelle architecture and water content should be considered when designing SEDDS-RMs for oral delivery.

The choice between dry and wet reverse micelles for oral drug delivery should be based on a multifactorial assessment of drug properties, formulation stability, and therapeutic goals. Hydrophilic payloads

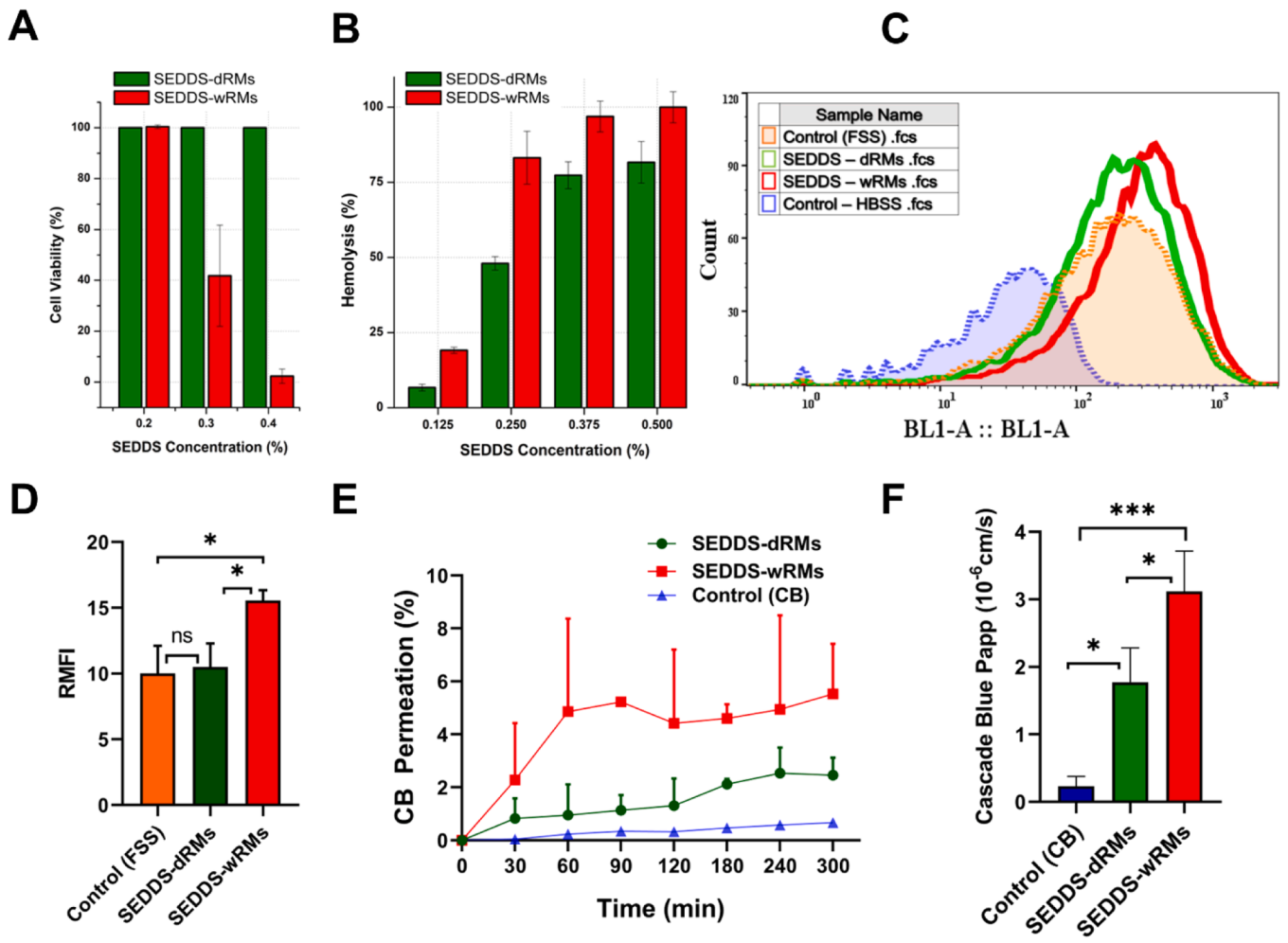


Fig. 6. Cell studies, A. Cell viability (%) of Caco-2 cells after incubation with indicated SEDDS emulsified in HBSS buffer in increasing concentrations at 37 °C for 3 h, B. Hemolysis [%] of erythrocytes after incubation with SEDDS-RMs in different concentrations for 3 h at 37 °C, C. Fluorescent shifts results of cellular uptake of FSS in SEDDS samples emulsified in HBSS buffer after incubation on Caco2-cells at 37 °C for 3 h, D. Cellular uptake is represented as relative mean fluorescent intensity (RMFI), E. Permeation of CB across Caco-2 cells at indicated time points during treatment with 0.2 % (m/v) SEDDS samples at 37 °C, F. Permeation of cascade blue in indicated formulations across Caco-2 monolayer, Data are shown as means ± SD ($n \geq 3$). Significant differences are indicated as * $p < 0.05$; ** $p < 0.01$; *** $p < 0.001$.

benefit from the aqueous cores of wRMs, but their lower stability may limit practical use in moisture-sensitive formulations. dRMs, on the other hand, demonstrate superior structural integrity and are especially suitable for lipophilic peptide complexes or drugs prone to hydrolysis. Additionally, factors like release kinetics, cytotoxicity thresholds, and manufacturing scalability should guide the formulation strategy. Supplementary Material Table S5 provides a practical selection matrix to guide formulation scientists in making such decisions.

3.5. *In vitro and in vivo HRP experiments*

The activity of HRP solubilized in reverse micelles was studied using OPD as the electron donor. HRP catalyzes the oxidation of OPD in the presence of H_2O_2, forming the chromogenic product 2,3-diaminophenazine (DAP) as shown in Fig. 7A. This product has a distinct yellow-orange color and absorbs light in the visible range. The intensity of the color is directly proportional to the concentration of H_2O_2 or OPD, allowing quantification of enzymatic activity. This reaction is commonly used to measure HRP activity in biochemical and analytical studies. This reaction is a key step in ELISAs, where HRP serves as a reporter enzyme for detecting specific antigens or antibodies.

Based on the molecular weight of HRP (44 kDa), the Stokes' radius was determined to be 2.7 nm. The theoretical average radius of the inner cavity of empty dry reverse micelles was calculated from Eq. (3) as 0.7 nm and 5.6 nm for wet reverse micelles. However, these reverse micelles are known to grow as they swell when loaded with molecules such as proteins. In a study, the radius before and after loading α-chymotrypsin into the reverse micelles formed with AOT and having different w_0 values was calculated. It was observed that when w_0 was 4, the radius of the reverse micelle was 6.55 nm before loading α-chymotrypsin and increased to 24.71 nm after loading [20]. Protein-loaded reverse micelles were generally observed to be larger in size compared to empty micelles, particularly at low w_0 values [43]. Maximum payload of the reverse micelles with HRP was determined by HPLC, and wRMs had a higher loading of 0.21 mg/g while dRMs had a loading of 0.01 mg/g (Fig. 7B). For both enzyme activity and pharmacokinetic evaluations, dRMs and wRMs were adjusted to an equivalent dose of HRP, allowing a fair comparison of delivery efficiency and stability without bias due to loading differences. This ensured that any observed differences were attributed to the formulation properties rather than variations in HRP payload. Since wet reverse micelles are larger than the protein, they provide sufficient free water to hydrate the enzyme. In many cases, enzyme activity in reverse micelles depends on water content, and maximum activity occurs when the enzyme size closely matches the available water pool [21]. Although wet reverse micelles have a higher payload capacity, the increased water content within their cores causes

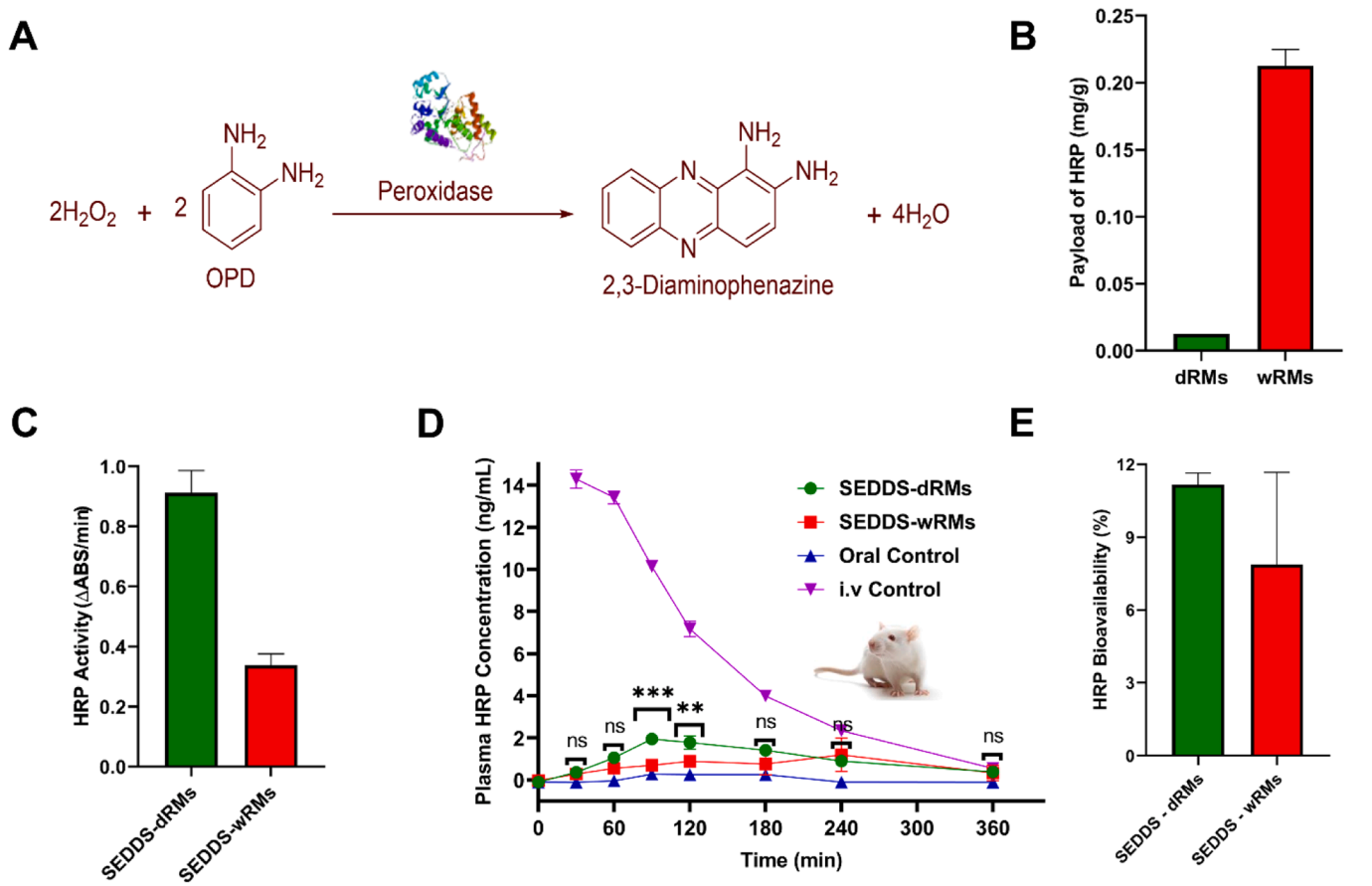


Fig. 7. Investigation of HRP activity in SEDDS formulations loaded with RMs, A. The mechanism of enzyme reaction for the measurement of *in vitro* HRP activity, B. The payload amount of HRP encapsulated in reverse micelles as determined by the HPLC, C. HRP enzymatic activity as a change in absorbance per unit of time, D. HRP blood profile measured using ELISA kit over time after oral administration to rats in solution in water (Oral Control) or encapsulation within SEDDS-dRMs and SEDDS wRMs, E. Bioavailability rates of HRP in rat blood administered by SEDDS containing reverse micelles. Data with different superscript stars (D) are significantly different ($p < 0.05$) according to ordinary two-way ANOVA test of individual variances by Sidak's multiple comparison test between SEDDS-dRMs and SEDDS-wRMs, Significant differences are indicated as * $p < 0.05$; ** $p < 0.01$; *** $p < 0.001$, ns: not significant.

dilution of hydrogen peroxide in the local microenvironment surrounding HRP. This reduction in substrate availability diminishes enzymatic activity, as demonstrated in Fig. 7C. Therefore, despite the higher loading capacity of wRMs, greater encapsulation does not necessarily lead to higher enzymatic performance. Conversely, dry reverse micelles lack a well-defined water pool or have a severely limited one, resulting in a more constrained and hydrophobic microenvironment. This environment enhances enzyme-substrate interactions by increasing local substrate concentration around the enzyme, thus optimizing enzymatic activity. Additionally, the reduced water content can help maintain the enzyme in a more catalytically active conformation. This confinement improves enzyme-substrate interactions, preserves enzyme structure, and maintains HRP in a catalytically favorable conformation. As a result, HRP encapsulated in dRMs retained higher enzymatic activity compared to wRMs. This highlights the importance of microenvironmental conditions over payload quantity in determining enzyme function in reverse micellar systems.

This is, to our knowledge, the first study to compare dRMs and wRMs under standardized payload conditions (*e.g.*, HRP-adjusted doses), enabling a fair comparison of *in vivo* absorption and enzymatic behavior. The pharmacokinetic parameters derived from the plasma HRP concentration-time profiles further support the *in vitro* enzyme activity findings (Fig. 7D). The peak plasma concentration and the area under the curve were both higher for the SEDDS-dRMs compared to the SEDDS-wRMs formulation.

The oral administration of SEDDS containing horseradish peroxidase-loaded reverse micelles demonstrated a significant effect on HRP bioavailability in rats. The bioavailability of HRP was quantified after oral administration of the formulations, and the results are summarized in Fig. 7E. SEDDS containing HRP-loaded dry reverse micelles exhibited a higher relative bioavailability, reaching 11.2 %. In contrast, the bioavailability of SEDDS containing HRP-loaded wet reverse micelles was lower, reaching 7.9 %. The results indicate a statistically significant yet modest difference in bioavailability between the two formulations. The improved performance of the dry reverse micelle formulation may be attributed to its increased stability and better encapsulation efficiency during the preparation process, as well as its ability to facilitate better protection of HRP from enzymatic degradation in the gastrointestinal environment. Conversely, the wet reverse micelle formulation, while effective in encapsulating HRP, may have been less efficient in protecting the enzyme under physiological conditions, leading to reduced bioavailability. These findings suggest that the dry reverse micelle-based SEDDS formulation could be a promising strategy for the oral delivery of HRP or similar therapeutic proteins, particularly where incremental increases in bioavailability are crucial (*e.g.*, for drugs with narrow therapeutic indices). These results align with previous studies on lipid-based formulations, where even minor improvements in bioavailability have been clinically significant for specific drug classes [44]. In a study, the *in vivo* blood exenatide bioavailability of RM/SEDDS was shown to be 11 % [45]. Although the 3.3 % higher bioavailability of dRMs over wRMs was statistically significant ($p < 0.05$), the clinical relevance of this difference may depend on additional factors such as

drug potency, therapeutic index, and patient variability. The translational impact of this difference warrants further investigation in disease models to assess its therapeutic relevance.

While this study demonstrates promising results for both dRMs and wRMs in enhancing the oral delivery of small molecules, several limitations should be acknowledged. First, the scalability of reverse micelle-based SEDDS remains a technical challenge, particularly for dRMs, which require precise control over surfactant ratios and phase behavior at low water content. Industrial-scale emulsification processes might require reformulation or process optimization to ensure consistency and reproducibility. Second, *in vivo* toxicity remains a concern, especially at higher emulsifier concentrations. Although cytotoxicity and hemolysis studies were performed *in vitro*, comprehensive long-term safety, immunogenicity, and biocompatibility evaluations in relevant animal models are crucial before clinical application. Third, while dRMs demonstrated superior enzymatic activity and modestly improved bioavailability compared to wRMs, their clinical useability will ultimately depend on drug-specific factors such as solubility, dosing frequency, and disease context. Moreover, in complex physiological environments, reverse micelle-based systems are likely to encounter additional challenges, such as enzymatic degradation in the gastrointestinal tract, mucus entrapment, and pH-dependent destabilization. These challenges may impair micelle integrity and drug release profiles, potentially limiting therapeutic effectiveness. Therefore, future research should also focus on optimizing the surface properties of reverse micelles, improving mucus penetration, and increasing enzyme resistance. Additional formulation efforts, especially those focusing on patient-centered factors (*e.g.*, taste-masking, capsule compatibility, excipient safety profiles), will be crucial for advancing these platforms toward clinical application.

4. Conclusions

In this study, we developed SEDDS formulations containing dry and wet reverse micelles with similar sizes, polydispersity indices, zeta potentials, and 24-hour stability, allowing for a fair comparison of their nanocarrier properties. Due to their ability to achieve higher logD values, improved encapsulation efficiency, and enhanced oral bioavailability of a model protein, dry reverse micelles are preferred over wet reverse micelles in SEDDS formulations. Generally, wRMs outperformed dRMs only in permeation studies. In wRMs, the dissolution of dye in the oily phase led to artificially higher apparent permeability, because dye molecules could permeate the membrane independently of micelle-mediated transport. Notably, SEDDS containing HRP-loaded dry reverse micelles achieved an oral bioavailability of 11.2 %, representing a significant 1.4-fold improvement compared to the SEDDS containing HRP-loaded wet reverse micelles. These findings suggest that dry reverse micelle-loaded SEDDS have significant potential for clinical use, providing a promising approach to enhance the oral bioavailability of drugs. Further research on the effects of different surfactants, oily phases, and the encapsulation methods on cellular uptake, permeability, and bioavailability is essential to improve dry reverse micelles for oral drug delivery. Such studies will be crucial in optimizing dry reverse micelles for oral drug delivery and broadening their use with a wider range of therapeutic agents.

CRediT authorship contribution statement

Numan Eczacioglu: Writing – review & editing, Writing – original draft, Visualization, Methodology, Investigation, Conceptualization. **Annika Postina:** Methodology, Investigation. **Melanie Ebert:** Methodology, Investigation. **Flavia Laffleur:** Methodology, Investigation. **Gergely Kali:** Methodology, Investigation. **Anna Seybold:** Methodology. **Andreas Bernkop-Schnürch:** Writing – review & editing, Writing – original draft, Supervision, Funding acquisition, Conceptualization.

Declaration of competing interest

The authors declare that they have no known competing financial interests or personal relationships that could have appeared to influence the work reported in this paper.

Acknowledgements

Numan Eczacioglu has received funding from the Scientific and Technological Research Council of Türkiye (TUBITAK), 2219-International Postdoctoral Research Fellowship Program (application no 1059B192202267). The authors are grateful to Assoc. Prof. Dr. Christoph Kreutz for his valuable help in the NMR measurements.

Data availability

Data will be made available on request.

Supplementary materials

Supplementary material associated with this article can be found, in the online version, at doi:10.1016/j.actbio.2025.07.027.

References

[1] T. Flanagan, Potential for pharmaceutical excipients to impact absorption: a mechanistic review for BCS class 1 and 3 drugs, Eur. J. Pharm. Biopharm. 141 (2019) 130–138, https://doi.org/10.1016/j.ejpb.2019.05.020.
[2] N. Samiei, S.M. Foroutan, F. Razipour, A. Zarghi, A. Shafaati, An investigation into the ability of alendronate ion pairs to increase oral absorption, Int. J. Pharm. 527 (2017) 184–190, https://doi.org/10.1016/j.ijpharm.2017.05.042.
[3] J.M. Miller, A. Dahan, D. Gupta, S. Varghese, G.L. Amidon, Quasi-equilibrium analysis of the ion-pair mediated membrane transport of low-permeability drugs, J. Control. Release 137 (2009) 31–37, https://doi.org/10.1016/j.jconrel.2009.02.018.
[4] O. Zupančič, A. Bernkop-Schnürch, Lipophilic peptide character – What oral barriers fear the most, J. Control. Release 255 (2017) 242–257, https://doi.org/10.1016/j.jconrel.2017.04.038.
[5] R. Bru, A. Sanchez-Ferrer, F. Garcia-Carmona, Kinetic models in reverse micelles, Biochem. J. 310 (1995) 721–739, https://doi.org/10.1042/bj3100721.
[6] R.S. Rahaman, J.Y. Chee, J.M.S. Cabral, T.A. Hatton, Recovery of an extracellular alkaline protease from whole fermentation broth using reversed micelles, Biotechnol. Prog. 4 (1988) 218–224, https://doi.org/10.1002/btpr.5420040405.
[7] P.L. Luisi, L.J. Magid, J.H. Fendler, Solubilization of enzymes and nucleic acids in hydrocarbon micellar solution, Crit. Rev. Biochem. Mol. Biol. 20 (1986) 409–474, https://doi.org/10.3109/10409238609081999.
[8] D.M. Zhu, K.I. Feng, Z.A. Schelly, Reverse micelles of triton X-100 in cyclohexane. Effects of temperature, water content, and salinity on the aggregation behavior, J. Phys. Chem. 96 (1992) 2382–2385, https://doi.org/10.1021/j100184a068.
[9] R. Urano, G.A. Pantelopulos, J.E. Straub, Aerosol-OT surfactant forms stable reverse micelles in apolar solvent in the absence of water, J. Phys. Chem. B 123 (2019) 2546–2557, https://doi.org/10.1021/acs.jpcb.8b07847.
[10] L. Chen, L. Mei, D. Feng, D. Huang, X. Tong, X. Pan, C. Zhu, C. Wu, Anhydrous reverse micelle lecithin nanoparticles/PLGA composite microspheres for long-term protein delivery with reduced initial burst, Colloids Surfaces B Biointerf. 163 (2018) 146–154, https://doi.org/10.1016/j.colsurfb.2017.12.040.
[11] M. Omidi, V. Mansouri, L. Mohammadi Amirabad, L. Tayebi, Impact of lipid/magnesium hydroxide hybrid nanoparticles on the stability of vascular endothelial growth factor-loaded PLGA microspheres, ACS Appl. Mater. Interfaces 13 (2021) 24370–24384, https://doi.org/10.1021/acsami.0c22140.
[12] T.L. Spehr, B. Frick, M. Zamponi, B. Stühn, Dynamics of water confined to reverse AOT micelles, Soft Matter 7 (2011) 5745–5755, https://doi.org/10.1039/c1sm05204g.
[13] E.L. Michor, B.S. Ponto, J.C. Berg, Effects of reverse micellar structure on the particle charging capabilities of the span surfactant series, Langmuir 32 (2016) 10328–10333, https://doi.org/10.1021/acs.langmuir.6b02959.
[14] G.G. Zampieri, H. Jäckle, P.L. Luisi, Determination of the structural parameters of reverse micelles after uptake of proteins, J. Phys. Chem. 90 (1986) 1849–1853, https://doi.org/10.1021/j100400a023.
[15] M.A. Luna, N.M. Correa, J.J. Silber, R.D. Falcone, F. Moyano, Properties of AOT reverse micelle interfaces with different polar solvents, J. Phys. Org. Chem. 29 (2016) 580–585, https://doi.org/10.1002/poc.3535.
[16] G. Eskici, P.H. Axelsen, The size of AOT reverse micelles, J. Phys. Chem. B 120 (2016) 11337–11347, https://doi.org/10.1021/acs.jpcb.6b06420.
[17] S. Haddadzadegan, F. Dorkoosh, A. Bernkop-Schnürch, Oral delivery of therapeutic peptides and proteins: technology landscape of lipid-based nanocarriers, Adv. Drug Deliv. Rev. 182 (2022) 114097, https://doi.org/10.1016/j.addr.2021.114097.

[18] A.M. Jörgensen, C. Steinbring, D. Stengel, D. To, P. Schmid, A. Bernkop-Schnürch, Self-emulsifying drug delivery systems (SEDDS) containing reverse micelles: advanced oral formulations for therapeutic peptides, Adv. Healthc. Mater. 12 (2023) 2302034, https://doi.org/10.1002/adhm.202302034.
[19] M. Sandmeier, F. Ricci, D. To, S. Lindner, D. Stengel, M. Schifferle, S. Koz, A. Bernkop-Schnürch, Design of self-emulsifying oral delivery systems for semaglutide: reverse micelles *versus* hydrophobic ion pairs, Drug Deliv. Transl. Res. 15 (2024) 2146–2161, https://doi.org/10.1007/s13346-024-01729-0.
[20] E. Ruckenstein, P. Karpe, On the enzymatic superactivity in ionic reverse micelles, J. Colloid Interface Sci. 139 (1990) 408–436, https://doi.org/10.1016/0021-9797(90)90115-5.
[21] A.M. Azevedo, L.P. Fonseca, D.L. Graham, J.M.S. Cabral, D.M.F. Prazeres, Behaviour of horseradish peroxidase in AOT reversed micelles, Biocatal. Biotransf. 19 (2001) 213–233, https://doi.org/10.3109/10242420109105265.
[22] P.L. Luisi, M. Giomini, M.P. Pileni, B.H. Robinson, Reverse micelles as hosts for proteins and small molecules, BBA - Rev. Biomembr. 947 (1988) 209–246, https://doi.org/10.1016/0304-4157(88)90025-1.
[23] G. Kali, A.H. Mayer, D. To, M. Truszkowska, A. Seybold, D.E. Braun, R. Plangger, M. Gallei, A. Bernkop-Schnürch, Polycaprolactone/α-cyclodextrin polyrotaxanes with cellular uptake enhancing properties, J. Mater. Chem. B 13 (2025) 3471–3482, https://doi.org/10.1039/D4TB02451F.
[24] T.N.Q. Phan, B. Le-Vinh, N.A. Efiana, A. Bernkop-Schnürch, Oral self-emulsifying delivery systems for systemic administration of therapeutic proteins: science fiction? J. Drug Target. 27 (2019) 1017–1024, https://doi.org/10.1080/1061186X.2019.1584200.
[25] O. Kaplan, M. Truszkowska, G. Kali, P. Knoll, M.B. Massani, D.E. Braun, A. Bernkop-Schnürch, Thiolated α-cyclodextrin: the likely smallest drug carrier providing enhanced cellular uptake and endosomal escape, Carbohydr. Polym. 316 (2023) 121070, https://doi.org/10.1016/j.carbpol.2023.121070.
[26] P. Knoll, G. Francesco Racaniello, V. Laquintana, F. Veider, A. Saleh, A. Seybold, N. Denora, A. Bernkop-Schnürch, Lipid-based nanoparticles: enhanced cellular uptake via surface thiolation, Int. J. Pharm. 635 (2023) 122753, https://doi.org/10.1016/j.ijpharm.2023.122753.
[27] E. Abuin, E. Lissi, R. Duarte, J.J. Silber, M.A. Biasutti, Solubilization in AOT- water reverse micelles. Effect of the external solvent, Langmuir 18 (2002) 8340–8344, https://doi.org/10.1021/la020492o.
[28] D.L. Gurina, Y.A. Budkov, Insights into the self-assembly of water reverse micelles and solubilization process in liquid and supercritical solvents: a molecular dynamics study, Colloids Surfaces A Physicochem. Eng. Asp. 676 (2023) 132200, https://doi.org/10.1016/j.colsurfa.2023.132200.
[29] S. Sharma, N. Yadav, P.K. Chowdhury, A.K. Ganguli, Controlling the microstructure of reverse micelles and their templating effect on shaping nanostructures, J. Phys. Chem. B 119 (2015) 11295–11306, https://doi.org/10.1021/acs.jpcb.5b03063.
[30] P. Rastogi, D. Honecker, D.A. Venero, N. Mahmoudi, N.S. Kaisare, M.G. Basavaraj, Modulating shape transition in surfactant stabilized reverse microemulsions, Soft Matter 19 (2023) 7033–7045, https://doi.org/10.1039/D3SM00682D.
[31] S. Taokaew, M. Ofuchi, T. Kobayashi, Size distribution and characteristics of chitin microgels prepared via emulsified reverse-micelles, Materials 12 (2019) 1160, https://doi.org/10.3390/ma12071160.
[32] Y. Zhao, J. Zhang, B. Han, C. Zhang, W. Li, X. Feng, M. Hou, G. Yang, Effect of compressed CO2 on the properties of Lecithin reverse micelles, Langmuir 24 (2008) 9328–9333, https://doi.org/10.1021/la801427b.
[33] M. Ueda, Z.A. Schelly, Mean aggregation number and water vapor pressure of aot reverse micellar systems determined by controlled partial pressure-vapor pressure osmometry (CPP-VPO), Langmuir 4 (1988) 653–655, https://doi.org/10.1021/la00081a026.
[34] K.E. Goklen, T.A. Hatton, Liquid-Liquid extraction of low molecular-weight proteins by selective solubilization in reversed micelles, Sep. Sci. Technol. 22 (1987) 831–841, https://doi.org/10.1080/01496398708068984.
[35] R.B.G. Wolbert, R. Hilhorst, G. Voskuilen, H. Nachtegaal, M. Dekker, K.V.T. Riet, B. H. Bijsterbosch, Protein transfer from an aqueous phase into reversed micelles: the effect of protein size and charge distribution, Eur. J. Biochem. 184 (1989) 627–633, https://doi.org/10.1111/j.1432-1033.1989.tb15059.x.
[36] S. Ichikawa, M. Imai, M. Shimizu, Solubilizing water involved in protein extraction using reversed micelles, Biotechnol. Bioeng. 39 (1992) 20–26, https://doi.org/10.1002/bit.260390105.
[37] M.J. Pires, M.R. Aires-Barros, J.M.S. Cabral, Liquid-liquid extraction of proteins with reversed micelles, Biotechnol. Prog. 12 (1996) 290–301, https://doi.org/10.1021/bp950050l.
[38] M. Zulauf, H.F. Eicke, Inverted micelles and microemulsions in the ternary system H2O/aerosol-OT/isooctane as studied by photon correlation spectroscopy, J. Phys. Chem. 83 (1979) 480–486, https://doi.org/10.1021/j100467a011.
[39] A. Siddiqa, M. Faisal, Heavy metals: source, toxicity mechanisms, health effects, nanotoxicology and their bioremediation, Contam. Agric. Sources, Impacts Manag. (2020) 117–141, https://doi.org/10.1007/978-3-030-41552-5_6.
[40] M. Yang, J. Bylund, Quantitative 3D imaging of living organs-on-chips with a high-speed point-scanning confocal system, Nat. Methods (2021).
[41] G. Mahajan, E. Doherty, T. To, A. Sutherland, J. Grant, A. Junaid, A. Gulati, N. LoGrande, Z. Izadifar, S.S. Timilsina, V. Horváth, R. Plebani, M. France, I. Hood-Pishchany, S. Rakoff-Nahoum, D.S. Kwon, G. Goyal, R. Prantil-Baun, J. Ravel, D. E. Ingber, Vaginal microbiome-host interactions modeled in a human vagina-on-a-chip, Microbiome 10 (2022) 1–18, https://doi.org/10.1186/s40168-022-01400-1.
[42] A. Herland, B.M. Maoz, D. Das, M.R. Somayaji, R. Prantil-baun, R. Novak, M. Cronce, T. Huffstater, S.S.F. Jeanty, M. Ingram, A. Chalkiadaki, D.B. Chou, S. Marquez, A. Delahanty, S. Jalili-firoozinezhad, Y. Milton, A. Sontheimer-phelps, B. Swenor, O. Levy, K.K. Parker, A. Przekwas, D.E. Ingber, Quantitative prediction of human pharmacokinetic responses to drugs via fluidically coupled vascularized organ chips Anna, Nat. Biomed. Eng. 4 (2020) 421–436, https://doi.org/10.1038/s41551-019-0498-9.
[43] S.F. Matzke, A.L. Creagh, C.A. Haynes, J.M. Prausnitz, H.W. Blanch, Mechanisms of protein solubilization in reverse micelles, Biotechnol. Bioeng. 40 (1992) 91–102, https://doi.org/10.1002/bit.260400114.
[44] D.V. Bhalani, B. Nutan, A. Kumar, A.K. Singh Chandel, Bioavailability enhancement techniques for poorly aqueous soluble drugs and therapeutics, Biomedicines 10 (2022) 2055, https://doi.org/10.3390/biomedicines10092055.
[45] M. Lin, L. Wu, Y. Lu, X. Bao, H. Zhong, Q. Dai, Q. Yang, Y. Xia, X. Tan, Y. Qin, R. Jiang, M. Han, Membrane fusion reverse micelle platforms as potential oral nanocarriers for efficient internalization of free hydrophilic peptides, Nano Res. 16 (2023) 9768–9780, https://doi.org/10.1007/s12274-023-5645-7.